Synthesis of CuO Nanorods, Reduction of CuO into Cu Nanorods, and Diffuse Reflectance Measurements of CuO and Cu Nanomaterials in the Near Infrared Region

Khadga M. Shrestha,[†] Christopher M. Sorensen,[‡] and Kenneth J. Klabunde*[,†]

Department of Chemistry and Department of Physics, Kansas State University, Manhattan, Kansas 66506

Received: April 26, 2010; Revised Manuscript Received: July 22, 2010

CuO nanorods were synthesized by hydrothermal methods with three different chemical combinations: (i) copper nitrate, lactic acid, and sodium hydroxide; (ii) copper sulfate, sodium lactate, and sodium hydroxide; and (iii) copper nitrate and sodium hydroxide. Physical parameters, concentration, temperature, and aging time, greatly affected the size and morphology of the nanorods; CuO nanoparticles were also prepared. These nanorods and nanoparticles were reduced to metallic copper at elevated temperature by 4% H_2 diluted in helium. The morphology of CuO nanomaterials (nanorods and nanoparticles) was preserved after reduction. These CuO and Cu nanorods and nanoparticles were characterized by XRD, SEM, TEM, SEM-EDS, and BET measurements. The CuO and Cu nanomaterials were employed for near-infrared (NIR) diffuse reflectance. Among these materials, CuO nanorods were to be found the best NIR diffuse reflectors, indicating potential application as NIR obscurants.

1. Introduction

Transitional metal oxides and metals are extensively used in various applications because of their specific catalytic, optical, electrical, and magnetic properties.[1,2] Among them, copper oxide (CuO) and copper metal are important materials; CuO is a p-type semiconductor, an antiferromagnetic material, and a high-temperature superconductor with a narrow band gap of 1.2 eV. It is used in batteries, gas sensing, magnetic storage media, and solar energy conversion.[3] On the other hand, copper metal is extensively used as a conductor in modern electronic circuits due to its excellent electrical conductivity and lower cost.[4]

It has been shown that nanomaterials have different optical, electrical and magnetic, and structural properties, depending upon size and morphology which are not fully explained by current theories.[5,6] There have been considerable efforts toward fabrication of CuO and Cu nanomaterials to enhance their existing applications. There are several reports on the synthesis of CuO nanomaterials with different morphologies—CuO nanoparticles,[7,8] nanocrystals,[9,10] nanowires,[11,12] and nanorods.[13,14] Nanoribbons and nanorings[15] and nanoflowers[16,17] have also been reported. Similarly, there are several reports about copper nanomaterials—nanowires,[18−20] nanorods,[21−23] and nanoparticles.[24−29]

The extinction of light by matter is a common phenomenon. The extent of extinction of light depends upon the nature of the material and the radiation. The extinction of infrared (IR) has a significant role in military applications as this is the basis of IR obscurants. IR wavelengths (0.5−15 μm, tactical IR wave band) are important in military applications because most observation technologies rely on sensors that are operated in this wave band.[30] IR obscurants play an important role in military operations because they provide protection of military personnel, equipment, and installations from IR-guided weapons.[31−33] In this context, certain nanomaterials might be excellent IR obscurants because they have the potential to enhance the IR extinction. Nanomaterials of some metal oxides give more diffuse reflectance (ratio of scattering coefficient to scattering coefficient plus absorption coefficient) than bulk materials at the near-infrared region (NIR).[34]

In this paper, we report the synthesis of CuO nanorods by novel routes. Moreover, we also synthesized spheroidal CuO nanoparticles. Then we reduced these CuO nanorods to Cu nanorods and CuO nanonoparticles to Cu nanoparticles with hydrogen. It is important to note that we were able to preserve the morphology of these CuO nanomaterials after reduction. To the best of our knowledge, this is the first report of reduction of CuO nanomaterials to form Cu nanomaterials while preserving the morphology. Ultimately, the purpose of investigating CuO and Cu nanomaterials (nanorods and nanoparticles) was to compare their diffuse reflectance properties in the NIR region. Experimentally, we found that CuO nanorods are better diffuse reflectors compared to all other CuO and Cu nanomaterials. This shows that at least one optical property depends upon the morphology of the CuO. This indicates that CuO nanorods might have potential as an IR obscurant.

2. Experimental Section

2.1. Synthesis of CuO Nanorods. All chemical reagents were of analytical grade and used without further purification. We synthesized CuO nanorods by three different chemical combinations.

(i) In the first case, CuO nanorods were synthesized using copper(II) nitrate solution in ethanol, aq solutions of NaOH, and lactic acid. In a particular experiment, 6 mL of 8.5% lactic acid in water and 3 mL of 0.5 M $Cu(NO_3)_2$ in ethanol were placed in a beaker and stirred vigorously; the solution was transferred to 100 mL Teflon-lined autoclave. Then 10 mL of 5 M NaOH was added; the reaction mixture was sealed in the stainless pressure container and kept for 24 h at 140 °C. Then it was cooled to room temperature. The product was washed with distilled water three times followed by ethanol and dried at 80 °C for three hours. The maximum yield of the product recovered was 78%.

(ii) In the second case, CuO nanorods were synthesized using $CuSO_4$, sodium lactate, and NaOH. During the synthesis, 0.5 g

* Corresponding author. E-mail: kenjk@ksu.edu.
[†] Department of Chemistry.
[‡] Department of Physics.

10.1021/jp103761h
Published on Web 08/06/2010

of copper(II) sulfate, and 0.45 g of sodium lactate were taken in a beaker containing 40 mL of water and stirred for 15 min. Then 0.24 g of NaOH was added and stirred for 1 h. Then the reaction mixture was transferred to a Teflon-lined stainless steel autoclave and sealed. The reaction mixture was kept for 24 h at 140 °C. The product was cooled to room temperature and washed with distilled water three times followed by ethanol. It was dried at 80 °C for three hours. The product was recovered, and the yield was 81%.

(iii) In the third case, a 0.5 M $Cu(NO_3)_2$ solution in ethanol and a 10 M aq solution of NaOH were prepared as stock solutions. In a particular experiment, a mixture of 1 mL of 0.5 M $Cu(NO_3)_2$ and 10 mL of 5 M NaOH was placed in a 100 mL Teflon-lined stainless steel autoclave and sealed. The reaction mixture was kept at different reaction conditions; the effects of NaOH concentration, aging times, and temperatures were studied. In all cases, the reactor was allowed to cool at room temperature. The product was washed with distilled water three times and with ethanol two times; it was dried at 80 °C for three hours. The yield of CuO product was up to 84% when measured for many experiments.

2.2. Reduction of CuO Nanomaterials into Cu Metal Nanorods and Nanoparticles. CuO nanomaterials (nanorods and nanoparticles) were reduced to corresponding Cu nanomaterials. In this process, CuO was placed into a small glass boat of 5 cm in length, 0.8 cm internal diameter, and 1 cm external diameter. The boat was inserted in the middle of a long glass tube (length = 30 cm, internal diameter = 1.2 cm) and supported with glass wool. The glass tube containing the sample boat equipped with a temperature monitor (sensor) was inserted in the cylindrical hole (diameter =1.5 cm) of a rectangular furnace (l = 20 cm, b = 6 cm, h = 7 cm). The temperature sensor was inserted between the cylindrical hole of the furnace and the glass tube near the sample. One end of the glass tube was connected with a plastic tube for incoming dilute H_2 gas, and the other end was connected with another tube for outgoing waste gas after reaction. Then 4% hydrogen gas diluted in helium was passed across the sample to drive out air for 10 min in the beginning. Then the furnace was heated electrically until the reduction temperature was attained with a continuous supply of the dilute H_2 gas, and the temperature was held for 1 h; the temperature was monitored with thermocouple. After the reduction of CuO into Cu, the product was cooled to room temperature with the continuous flow of the mixture of gases. Furthermore, CuO nanoparticles (two different sizes) were synthesized by two reported methods and they were reduced to Cu nanoparticles.

2.3. Characterization. ***2.3.1. Powder X-ray Diffraction (XRD).*** The prepared CuO and Cu nanomaterials were investigated by powder X-ray diffraction. The instrument was a Scintag XDS 2000 spectrometer. The light source was Cu Kα radiation with applied voltage of 40 kV and current of 40 mA.

2.3.2. Scanning Electron Microscopy (SEM) and Transmission Electron Microscopy (TEM). The morphologies of the synthesized nanomaterials were observed by Scanning Electron Microscopy (SEM) and Transmission Electron Microscopy (TEM). SEM experiments were carried out by using a Scanning Electron Microscope-S3500N, Hitachi Science System, Ltd. at the Entomology Department of Kansas State University (KSU), microscopy and imaging facility. Some CuO and Cu nanomaterials were imaged with a transmission electron microscope, CM 100, Phillips at the biology department of KSU.

2.3.3. Brunauer−Emmet−Teller (BET) Measurements. Surface area, pore volume, and pore diameter of CuO and Cu nanomaterials were measured by using BET methods. The measurements were carried out using Microsorb II 2300 and Quantachrome NOVA 1200 instrumentation. The samples were cooled to 77 K using liquid nitrogen during the measurement.

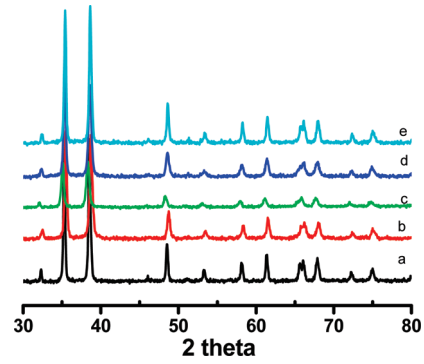

Figure 1. Powder XRD patterns of (a) spherical assemblies of CuO nanorods synthesized using $Cu(NO_3)_2$, lactic acid, and NaOH; (b) CuO nanorods synthesized using $Cu(NO_3)_2$, sodium lactate, and NaOH; (c) CuO nanoribbons and nanowires synthesized at room temperature in 24 h using 0.5 M $Cu(NO_3)_2$ and 5 M NaOH; (d) CuO nanorods synthesized at 140 °C in 24 h using 0.5 M $Cu(NO_3)_2$ and 5 M NaOH; (e) CuO nanorods synthesized at 140 °C in 24 h using 0.5 M $Cu(NO_3)_2$ and 7.5 M NaOH.

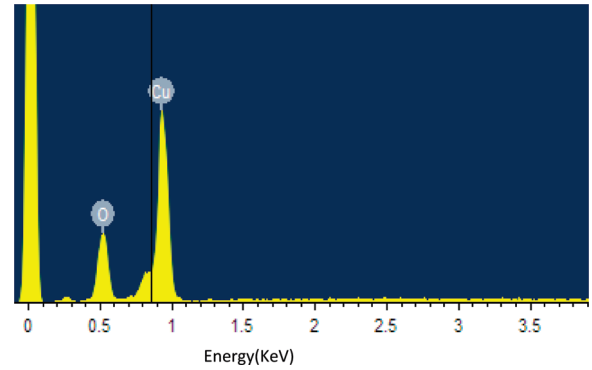

Figure 2. SEM-EDS element analysis for CuO nanorods synthesized at 140 °C in 24 h using 0.5 M $Cu(NO_3)_2$ and 5 M NaOH.

2.3.4. Measurement of Diffuse Reflectance at NIR by CuO and Cu Nanomaterials. The synthesized CuO and Cu nanomaterials (nanorods and nanoparticles) were used for NIR diffuse reflectance; it was determined with measuring diffuse reflectance as the function of wavelength. A Cary 500 UV−vis−NIR spectrometer with diffuse reflectance accessories (DRA) was used in the range of 900−1800 nm. The sample cell was made of two transparent CaF_2 discs, a Teflon O-ring and screw-type combination in which nanomaterials were packed between two discs and an O-ring. Polytetrafluoroethylene (PTFE) powder of 1 μm particle size was taken as a reference material.

3. Results and Discussion

3.1. CuO Nanorod Synthesis. CuO nanorods were synthesized by three chemical combinations. In the first case, we used copper nitrate, lactic acid, and sodium hydroxide. The reaction mixture appeared deep blue due to formation of copper lactate; copper hydroxide was formed by the reaction between the copper lactate and sodium hydroxide, and CuO nanorods were obtained upon decomposition of the copper hydroxide. Figure 1a shows the XRD pattern, and Figure 2 shows the SEM−EDS elemental analysis of the product; the XRD pattern confirms the formation of CuO, and the elemental analysis shows 1:1

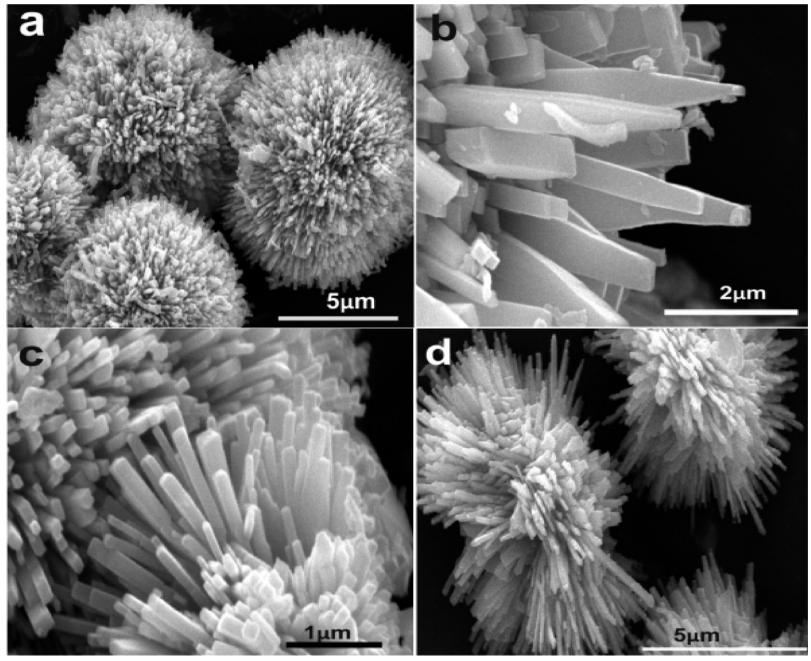

Figure 3. Spherical assemblies of CuO nanorods synthesized using copper nitrate, lactic acid, and sodium hydroxide in 24 h (a−c) at 140 °C (d) at 150 °C.

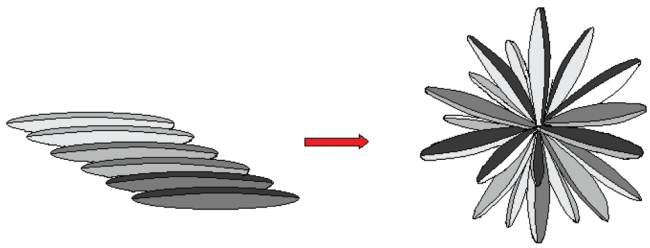

Figure 4. Proposed scheme for spherical assemblies of CuO nanorods.

ratio of copper and oxygen. SEM images (Figure 3a−c) show spherical assemblies of the nanorods synthesized at 140 °C; the diameter of a spherical assembly is up to 11 μm. The spherical assembly consists of rectangular rods with thickness 20−150 nm and breadth 100−200 nm. There was no separation of individual rods since they firmly assembled in the spherical structure. However, the nanorods synthesized at 150 °C (Figure 3d) were assembled loosely in an elliptical fashion. There were also separate individual rods, and the length was found to be up to 11 μm and thickness 50−200 nm. When synthesized at 150 °C, thickness and breadth of the rods were found to be shortened. The end sides of the rods were tapered with a little curvature that helped to form the spherical assemblies of nanorods. In some cases, hundreds of nanorods combined together to give a dense array. The proposed scheme for the spherical assembly is described by Figure 4.

In the second case, we synthesized the copper nanorods by using copper(II) sulfate, sodium lactate, and sodium hydroxide. Copper sulfate and sodium lactate react to give copper lactate. Copper lactate reacts with sodium hydroxide to give copper hydroxide which under decomposition gives CuO nanorods; the formation of CuO was confirmed by XRD (Figure 1b). SEM images a and b of Figure 5 show CuO nanorods synthesized at 140 and 150 °C, respectively. There was no significant difference in the morphology when they were synthesized at two different temperatures. Figure 5c shows the electron diffraction pattern of the CuO nanorods (Figure 5a). During the reaction, the formation of CuO can be illustrated by the following steps.

$$Cu^{2+} + \text{lactate} \rightarrow [Cu^{2+}\text{-lactate}]$$

$$[Cu^{2+}\text{-lactate}] + OH^{-} \rightarrow Cu(OH)_2$$

$$Cu(OH)_2 \rightarrow CuO + H_2O$$

In the third case, CuO nanorods were synthesized using an aqueous solution of sodium hydroxide and an ethanol solution of copper(II) nitrate; we carried out various sets of experiments changing temperature, concentration, aging time, and precursors so as to get optimum conditions for CuO nanorod synthesis, and studied the effects of these parameters on the morphology.

3.2. Effect of Temperature. First, we mixed alcoholic solutions with 5 M NaOH, and experiments were carried out for 24 h at various temperatures. The formation of CuO at room temperature was confirmed by XRD (Figure 1c) in the form of nanoribbons and nanowires (Figure 6a). When the same reaction was carried out for 96 h, there were transitions of nanoribbons to nanoplates, and nanowires to nanorods (Figure 6b). When the reaction was carried out for 24 h at 100 °C, most CuO nanomaterials were thin rectangular nanoplates with a small number of nanorods (Figure 6c). As the temperature was increased to 120 °C, most of the nanoplates were converted to nanorods with a rectangular cross section (thickness 40 to 150 nm). The length of the nanorods was found to be up to 2.8 μm (Figure 6d). When the same experiment was carried out at 140 °C, we found all nanorods with similar structure (Figure 6e). Figure 1d shows the XRD pattern of CuO synthesized at this condition. These nanorods had both rectangular and square cross sections, with length, breadth, and thickness in the range of 1.5−3.2 μm, 230−500 nm, and 80−200 nm, respectively. When the experiment was carried out at 150 °C, all the nanorods were made of nearly square cross section with sides of 250−650 nm and length up to 2.5 μm (Figure 6f). In general, when the temperature was increased, the nanorods were found to be shortened and thickened. When the experiment was at 160 °C, nanorods were found to be broken down. On the basis of these

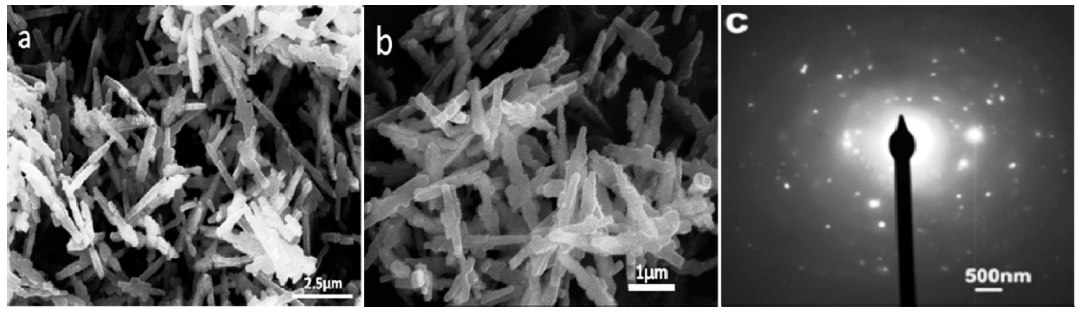

Figure 5. CuO nanorods synthesized using copper nitrate, sodium lactate, and sodium hydroxide for 24 h (a) at 140 °C, (b) at 150 °C; (c) electron diffraction pattern of CuO nanorods shown in (a).

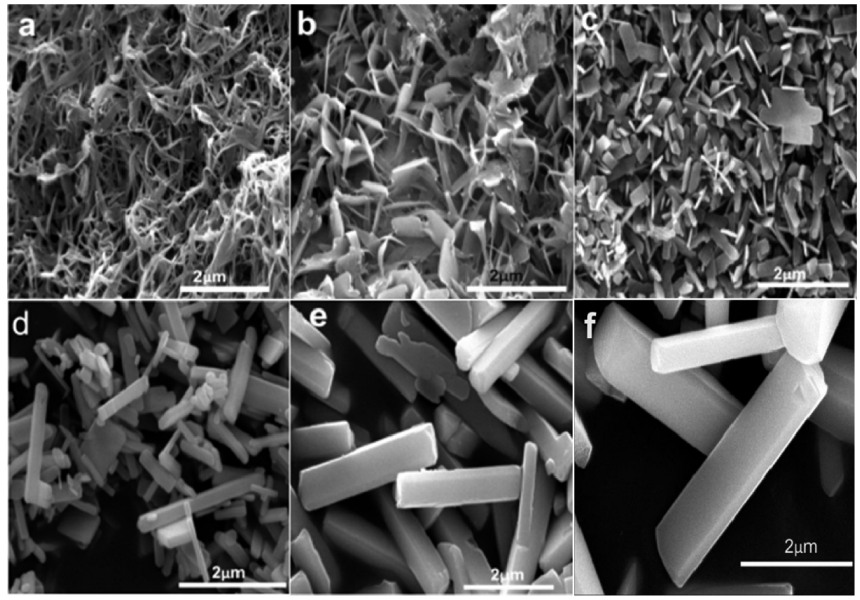

Figure 6. SEM images of CuO nanomaterials synthesized using copper nitrate and sodium hydroxide. (a) CuO nanoribbons and nanowires at room temperature in 24 h; (b) conversion of CuO nanoribbons to nanoplates, and nanowires to nanorods in 96 h at room temperature; (c) CuO nanorods and rectangular nanoplates at 100 °C in 24 h; (d) CuO nanorods at 120 °C in 24 h; (e) CuO nanorods at 140 °C in 24 h; (f) CuO nanorods at 150 °C in 24 h.

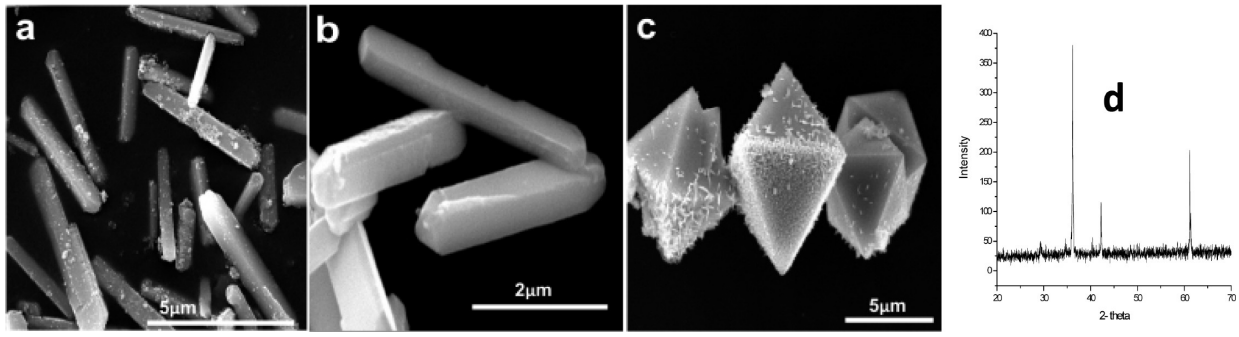

Figure 7. (a) CuO nanorods synthesized using 6.5 M NaOH and 0.5 M $Cu(NO_3)_2$ at 140 °C for 24 h. (b) CuO nanorods synthesized using 7.5 M NaOH and 0.5 M $Cu(NO_3)_2$ at 140 °C for 24 h. (c) Octahedrons of CuO and Cu_2O composite synthesized using 10 M NaOH and 0.5 M $Cu(NO_3)_2$ at 140 °C for 24 h. (d) XRD pattern of the octahedrons of CuO and Cu_2O composite.

experiments, the proper temperatures for the synthesis of CuO nanorods were between 140 and 150 °C.

3.2.1. Effect of NaOH Concentration. We also studied the effects of concentration of NaOH on the morphologies of CuO nanomaterials at 140 °C, keeping other parameters the same. We used 2.5, 5.0, 6.5, 7.5, and 10.0 M sodium hydroxide solutions. At the lower concentration of NaOH (2.5 M), most CuO nanomaterials were in the rectangular form, and only a few were in the form of nanorods. When the concentration of NaOH was increased, the thickness of the nanorods was found to be increased. CuO nanorods with rectangular and square cross sections were found by using 5 M NaOH (Figure 6e). When 6.5 and 7.5 M NaOH were used, CuO nanorods with square and almost circular cross sections were formed (Figure 7a−b). The formation of CuO using 7.5 M NaOH was confirmed by XRD (Figure 1e). However, when 10 M NaOH was used, we observed a composite of Cu_2O and CuO with octahedral structure (Figure 7c) instead of CuO nanorods. The formation of the composite was confirmed by XRD (Figure 7d). Some nanorods were distributed over the surface of the octahedral structure (Figure 7c). The XRD pattern (Figure 7d) shows that the main constituent of the octahedral structure was Cu_2O with

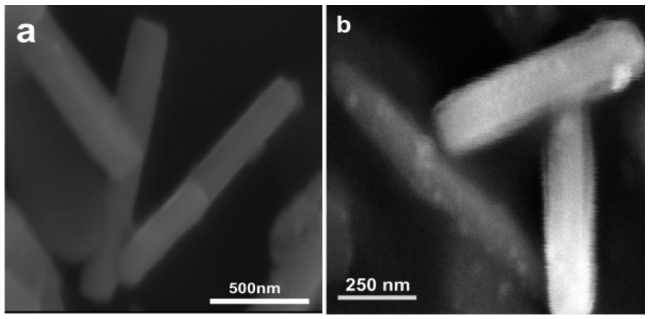

Figure 8. CuO nanorods synthesized using (a) $CuCl_2$ and (b) $(CH_3COO)_2Cu$ as Cu precursors.

a small amount of CuO. The major axis of the octahedron was found to be 6.7−10 μm. Apparently CuO was reduced to Cu_2O with ethanol used in the experiment.

3.2.2. Effects of Different Precursors. In addition to $Cu(NO_3)_2$, we used $CuCl_2$ and $(CH_3COO)_2Cu$ at 140 °C for 24 h. We obtained CuO nanorods in all cases, and there were no significant changes in the morphology of the nanorods (Figure 8a and b). However, we observed relatively shorter nanorods from $CuCl_2$ and $(CH_3COO)_2Cu$.

3.2.3. Effects of Aging Periods. We also studied the effects of aging times, while keeping the other parameters the same. In this set of experiments, we used 1 mL of 0.5 M $Cu(NO_3)_2$ and 10 mL of 5 M NaOH at 140 °C. We carried out experiments for 12, 24, 48, and 72 h. As we increased the aging time, the thickness of the nanorods was found to be increasing continuously; we can clearly observe the effects by comparing Figures 9a−c, and 6e. From the different sets of experiments, we found the following optimum conditions for the synthesis of CuO nanorods using Cu precursors in ethanol and aqueous solution of NaOH: (a) temperature - 140−150 °C, (b) NaOH concentration - 5.0−7.5 M, (c) aging time - 24 h, and (d) copper precursor - $Cu(NO_3)_2$.

When the $Cu(NO_3)_2$ solution was treated with concentrated sodium hydroxide, a blue precipitate was formed immediately. The blue precipitate turned black after a couple of minutes. The SEM image of the black product formed at 24 h by the reaction between NaOH and $Cu(NO_3)_2$ at room temperature shows long CuO chains (nanoribbons and nanowires) with width (30−160) nm (Figure 6a). As the aging time was increased up to 96 h at room temperature with the same composition, these long chains of CuO were thickened and shortened, and a few started to break (Figure 6b). The long chains (nanoribbons or nanowires) on treating at 100 °C were converted to CuO nanoplates or nanorods completely (Figure 6c). On further treatment above 100 °C, rectangular nanoplates were converted into nanorods with various dimensions.

3.3. Reduction of CuO Nanomaterials to Cu Nanomaterials. Literature teaches that there are many methods for the synthesis of CuO nanomaterials but there are limited methods for the preparation of Cu nanomaterials. We investigated methods to reduce CuO nanomaterials to Cu nanomaterials while preserving the morphology. Among the methods, we tried hydrogen gas under specific conditions to reduce CuO to Cu.[35] During our experiments, we used 4% H_2 gas diluted in helium at 285 °C for the reduction. Before raising the temperature, air was driven out using a mixture of helium and hydrogen gas. Then the temperature was raised electrically at the rate of 6 °C min^{-1} until 285 °C was attained with a continuous supply of hydrogen/helium gas at a flow rate of 240 mL min^{-1}. We passed the gas mixture for one hour at 285 °C and then turned off the heat. The hot product was allowed to cool with a continuous supply of the dilute hydrogen gas until room temperature was attained so that copper product could be prevented from aerial oxidation above room temperature. The XRD patterns of Cu products are shown in Figure 10a−d, which confirm the reduction of all the CuO materials to copper metal; Cu_2O as a transient intermediate that depends upon experimental conditions during the reduction may or may not be formed.[35,44] SEM images (Figure 11a−f) show the reduction of CuO nanorods to Cu nanorods with preserving the morphology.

$$CuO + H_2 \rightarrow Cu + H_2O$$

Panels a and b of Figure 11 are SEM images of Cu nanorods obtained by reduction of the spherical assembly of CuO as described for Figure 3a−c; the reduction was confirmed by the XRD pattern (Figure 10b). Figure 11c shows the SEM images of Cu nanorods obtained on reduction of CuO nanorods as described for Figure 5a; and Figure 11d,e are SEM images of Cu nanorods obtained on reduction of CuO nanorod samples as described for Figure 7b; the reduction was confirmed by XRD pattern (Figure 10c). Figure 11f is a SEM image of Cu nanorods obtained when the reduction was carried out at 295 °C by passing the dilute H_2 gas with the flow rate of 280 mL min^{-1} for CuO nanorod samples as described in Figure 7b. Moreover, CuO porous particles with diameter of 2−3.8 μm were prepared by a reported method[36] (Figure 12a,b). They were reduced to porous Cu particles (Figure 12c,d) under the same conditions as for the reduction of CuO nanorods, and the reduction was confirmed by the XRD pattern (Figure 10a). Smaller nanoparticles with diameter 8−10 nm were also synthesized by another reported method[37] (Figure 13a). Then the CuO nanoparticles were reduced to corresponding Cu nanoparticles (Figure 13b) under the same conditions as previously described; the formation of the nanoparticles was confirmed by XRD pattern (Figure 10d).

The important aspect of this reduction method is the absence of solvent since the reduction is carried out in a one-step gas−solid-phase reaction. The main achievement is to preserve the morphology of nanomaterials after reduction. However, we observed a slight decrease in the thickness of the nanorods and creation of a rough surface after reduction; the distortion was further enhanced when reduction was carried out at a higher rate flow (280 mL min^{-1}) of the H_2/He mixture *at 295°C*. The decrease in the thickness of nanorods is probably due to the lattice transition from monoclinic CuO nanorods to the more compact face-centered cubic Cu nanorods. In general, the thickness of the CuO nanorods or diameter of particles was found to be decreased by 10−15% during the reduction at 285 °C and 240 mL rate flow of H_2. The lattice change would induce the strain, and slower reduction was found to be more favorable to preserve the morphology. The rough surface of the Cu nanorods might be given by expulsion of water from the inner part of the nanorods especially at relatively higher temperature and rate flow of H_2.

3.4. BET Measurement. Some CuO and Cu nanoparticles and nanorods were examined by BET measurements. During the measurement, we took 150 ± 10 mg of CuO and Cu nanomaterials. As expected, the surface area of the small nanoparticles (9−10 nm) was found to be relatively greater (58 ± 6 m^2/g), and that of the larger porous particles was lower (5 ± 2 m^2/g). Similarly the surface area of a sample of CuO nanorods, which are larger in size than the smaller nanoparticles as described above, has lower suface area (5.2 ± 0.5 m^2/g, 9.2

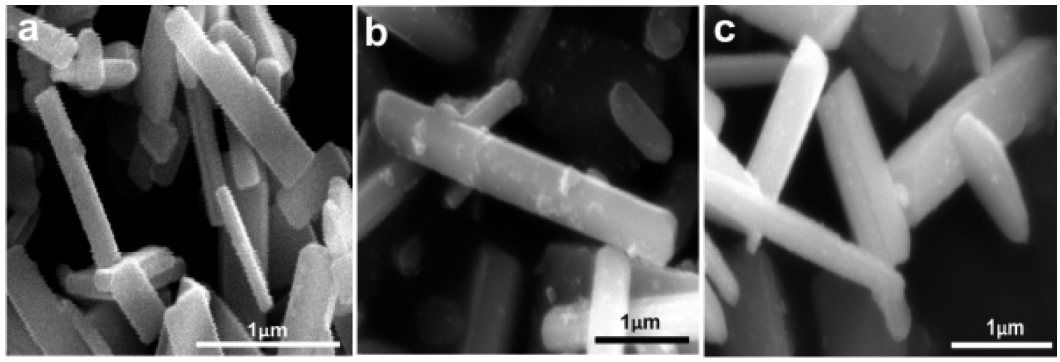

Figure 9. CuO nanorods synthesized at 140 °C using NaOH and $Cu(NO_3)_2$ for (a) 12, (b) 48, and (c) 96 h.

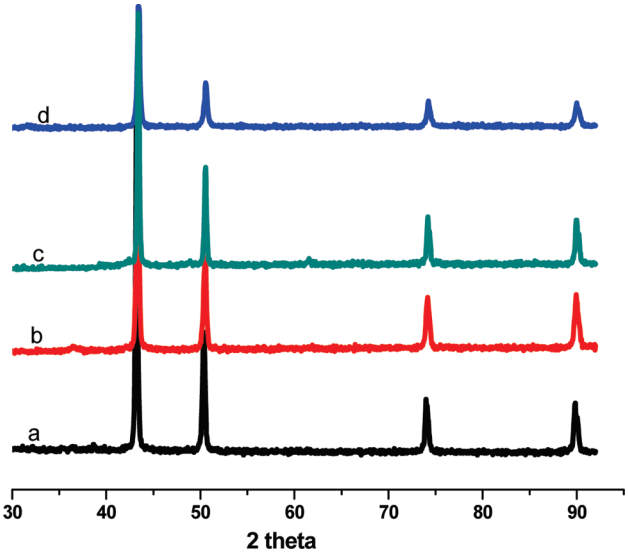

Figure 10. XRD pattern for (a) Cu porous particles (Figure 12c,d). (b) Cu nanorods assembled spherically (Figure 11a). (c) Cu nanorods (Figure 11d). (d) Cu nanoparticles (Figure 13b).

$\pm$ 0.5 m^2/g). In general, the surface areas of all CuO nanomaterials were found to be relatively small since they were prepared by a hydrothermal process. After reduction, the corresponding surface area for each Cu nanomaterial was found to be lower. The decrease in surface area after reduction is possibly due to sintering when CuO is reduced at high temperature. The surface areas, pore volumes, and pore diameters of various CuO and Cu samples with error data have been shown in Table 1.

3.5. Comparative Study of Diffuse Reflection at NIR by CuO and Cu Nanomaterials. The CuO and Cu nanomaterials can be used in different applications; in particular, CuO can used as a catalyst,[43−46] and Cu can be used as a sensor on the basis of its metallic plasmon resonance properties.[47−49] However, our main interest was to investigate their NIR diffuse reflectance properties based on their morphologies.

When a beam of radiation strikes an object, absorption, reflection, and transmission take place. Light is extinguished either by absorption or scattering.[38] The extent of these phenomena depends upon the nature of material, particle size, surface, and wavelength of radiation. If a sample is optically thick enough, no transmitted light is possible; thus, light is either absorbed or reflected by the sample. If a sample weakly absorbs, most of the light is reflected. So when a NIR beam strikes a weakly absorbing media without transmission, the radiation penetrates the medium up to a certain thickness. The beam changes its direction due to reflection, refraction, and random

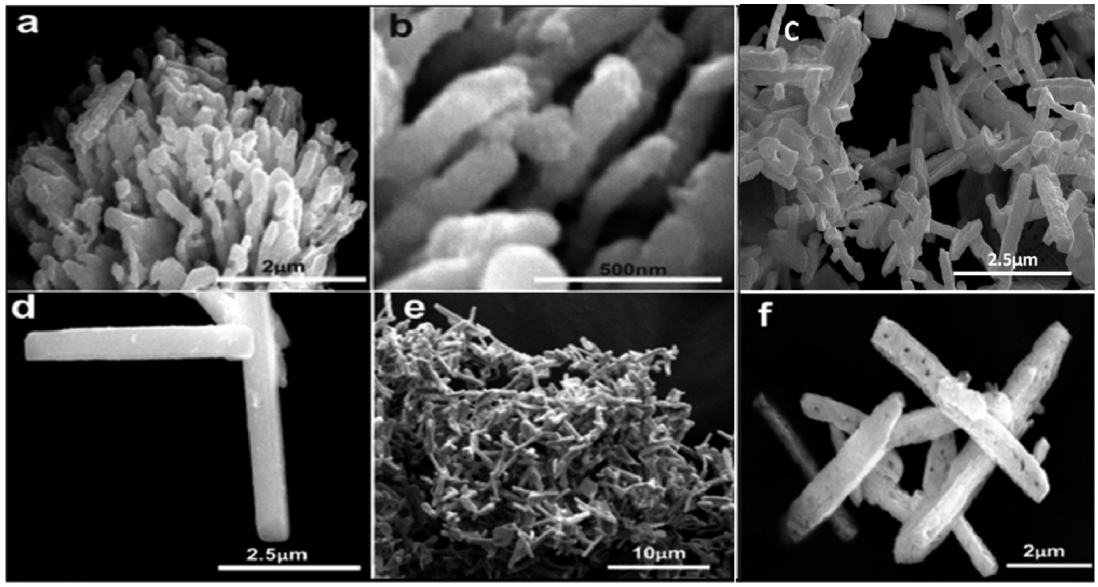

Figure 11. SEM images of (a,b). Spherical assemblies of Cu nanorods obtained by reducing CuO nanorods as described for a−c of Figure 3. (c) Cu nanorods obtained by reducing CuO nanorods as described for Figure 5a. (d) Cu nanorods obtained by reducing CuO nanorods as described for Figure 7b at 285 °C at a flow rate of 240 mL min^{-1}. (e) Cu nanorods at lower magnification obtained by reducing CuO nanorods as described for Figure 7a. (f) Cu nanorods obtained by reducing CuO nanorods as described for Figure 7a at 295 °C at the rate flow of 260 mL min^{-1}.

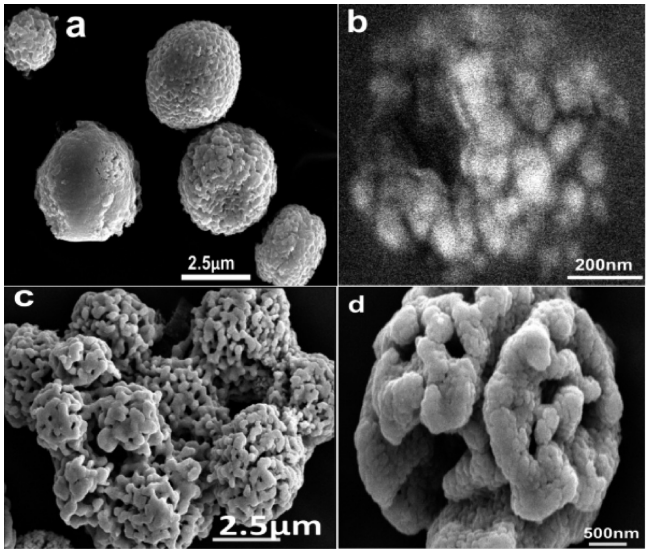

Figure 12. (a,b) CuO porous particles by decomposition of copper oxalate, (c,d) Cu porous particles by reducing the porous CuO particles (in a,b).

diffraction at the surfaces of various particles. The combination of all these effects is called diffuse light scattering.[39]

Previously, the diffuse reflectance of NIR from various metal oxide nanoparticles and corresponding bulk material has been compared in our laboratory; metal oxide nanoparticles have the ability to diffusely reflect more NIR (~15−20%) than the corresponding bulk material.[34] Then our interest was to study how the change of morphology of the same nanomaterial affects NIR diffuse reflectance.

The diffuse reflectance of NIR by samples of CuO and Cu as described above were measured; powdered CuO and Cu nanorods (length = 2.7−5.4 μm, sides = 250−600 nm) and CuO nanoparticles of two different sizes (porous particles with diameter = 2−3.8 μm; smaller particles with diameter = 8−10 nm) were employed during measurements. About (300 ± 10 mg) of each sample was taken in a sample holder so as to get a sufficient optical thickness to prevent transmission of the NIR. The measurement was carried out using a Cary 500 UV−vis−NIR spectrophotometer along the diffuse reflectance accessory (DRA). The measurement was carried out in a NIR region (wavelength range 900−1800 nm) in diffuse reflectance mode. Polytetrafluoroethylene (PTFE) powder (Aldrich, particle size ~1 μm) was taken as a reference sample for the normalization of diffuse reflectance of CuO and Cu materials. The reproducibility limit was within ±5%. Considering that there might

TABLE 1: Surface Area, Pore Volume, and Pore Diameter of Different CuO and Cu Nanomaterials

sample no.[a]	samples	BET surface area (m^2/g)	pore volume (cc/g)	pore diameter (nm)
1	CuO nanorods (Figure 7b)	5.2 ± 0.5	0.020 ± 0.010	2.4 ± 0.5
2	CuO nanorods (Figure 5b)	9.3 ± 0.5	0.030 ± 0.010	2.1 ± 0.2
3	CuO NPs (Figure 12a)	5 ± 2	0.023 ± 0.007	2.9 ± 0.9
4	CuO NPs (Figure 13a)	58 ± 6	0.128 ± 0.001	5.6 ± 0.0
5	Cu NRs (Figure 11c)	1.3 ± 0.3	0.006 ± 0.002	2.9 ± 0.8
6	Cu NRs (Figure 11d)	1.9 ± 0.3	0.007 ± 0.002	2.4 ± 0.4
7	Cu NPs (Figure 13b)	5.2 ± 0.3	0.033 ± 0.001	3.8 ± 0.0

[a] Sample 1: the CuO nanorods as described for Figure 7b. (2) Sample 2: the CuO nanorods as described for Figure 5b. (3) Sample 3: the porous nanoparticles as described for Figure 12a. (4) Sample 4: the CuO nanoparticles as described for Figure 13a. (5) Sample 5: Cu nanorods obtained by reduction of sample 1. (6) Sample 6: the Cu nanorods obtained reduction of sample 2. (7) Sample 7: Cu nanoparticles obtained by reduction of sample 4.

be some adsorbate on the surface of the CuO and Cu samples that might affect the diffuse reflectance of NIR, all these samples were heated at 130 °C so as to remove volatile adsorbates, such as water. After cooling, diffuse reflectance of NIR were measured immediately, and showed no significant differences for corresponding samples before and after heating; the differences were within the range of ±4.

Figure 15 shows NIR diffuse reflectance curves (diffuse reflectance vs wavelength) for different samples. CuO nanorods have the highest diffuse reflectance (Figure 15a) and, relatively shorter and thinner CuO nanorods (Figure 15b) gave slightly less diffuse reflectance. The diffuse reflectance of smaller nanoparticles (8−10 nm) is less than the diffuse reflectance given by both types of nanorods but greater than diffuse reflectance (Figure 15e) given by bigger porous nanoparticles (diameter = 2−3.8 μm). The commercial CuO particles (Figure 14) diffused the least amount of NIR (Figure 15h). CuO nanorods are good diffuse reflectors among other CuO materials (nanoparticles and commercial CuO bulk powders); however, Cu nanomaterials are poor diffuse reflectors (Figure 15 f,g,i). The sample which reflects less NIR absorbs more, so that Cu nanomaterials are good NIR absorbers. To understand and compare clearly, the diffuse reflectance given

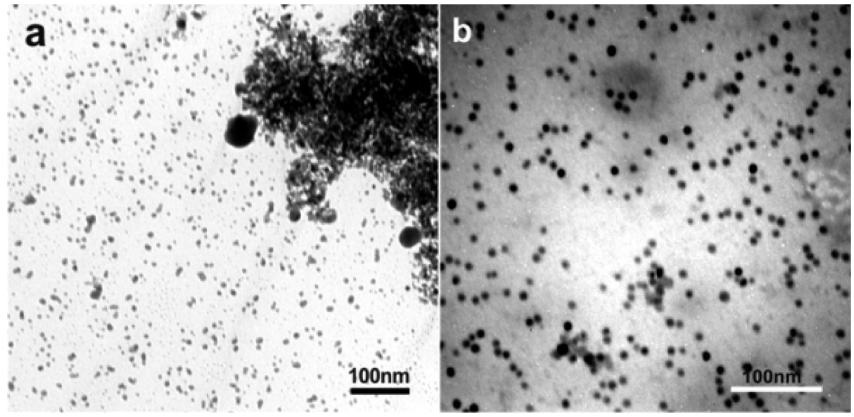

Figure 13. (a) CuO nanoparticles prepared by the reaction between copper acetate and alcohol. (b) Cu nanoparticles obtained by reducing the CuO nanoparticles (in a).

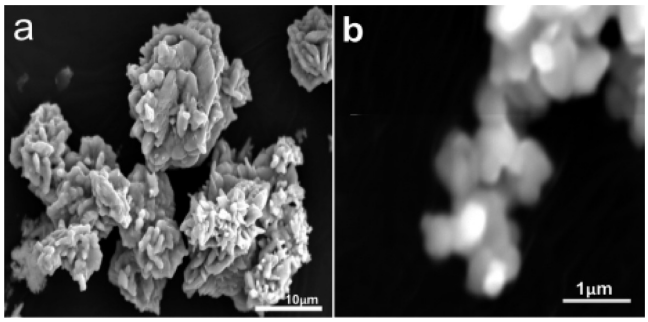

Figure 14. SEM images of commercial CuO bulk particles.

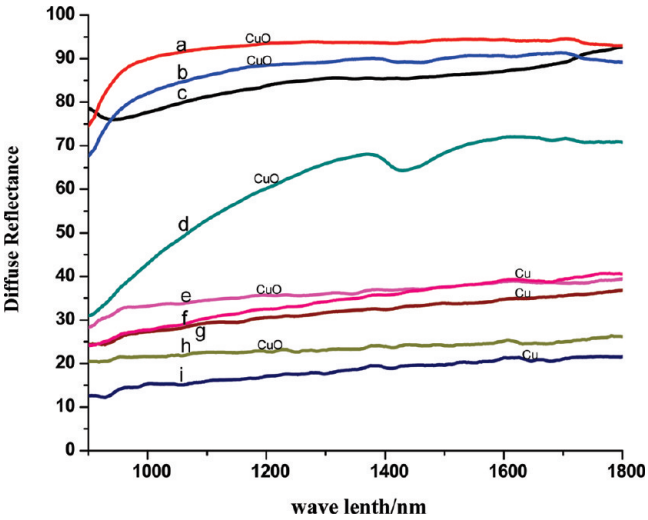

Figure 15. Diffuse reflectance curves at NIR given by (a) CuO nanorods as described for Figure 7b; (b) CuO nanorods as described for Figure 6e; (c) PTFE as reference material; (d) CuO nanoparticles as described for Figure 13a; (e) CuO porous particles as described for Figure 12a,b; (f) Cu porous particles as described for Figure 12c,d; (g) Cu nanoparticles as described for Figure 13b; (h) CuO commercial bulk particles; (i) Cu nanorods as described for Figure 11d,e.

TABLE 2: Diffuse Reflectance of Various CuO and Cu Materials at 1000, 1400, and 1800 nm

samples - curves	R^a at 1000 nm	R^a at 1400 nm	R^a at 1800 nm
CuO NRs[b] - Figure 15a	88 ± 3	91 ± 3	90 ± 3
CuO NRs[b] - Figure 15b	80 ± 3	87 ± 4	86 ± 4
CuO NPs[c] (nm) - Figure 15d	49 ± 5	68 ± 1	71 ± 1
CuO NPs[c] (μm) - Figure 15e	32 ± 2	37 ± 1	38 ± 3
CuO (CM[d]) - Figure 15h	21 ± 1	25 ± 1	27 ± 0
Cu NRs[b] - Figure 15i	14 ± 1	19 ± 2	20 ± 1
Cu NPs[c] (nm) - Figure 15g	27 ± 1	32 ± 1	35 ± 2
Cu NPs[c] (μm) - Figure 15f	32 ± 4	38 ± 1	38 ± 1

[a] *R*: diffuse reflectance, NRs. [b] Nanorods, NPs. [c] Nanoparticles, CM. [d] Commercial.

by all CuO and Cu materials with error data at three particular wavelengths has been presented in the Table 2.

Diffuse scattering of light by complex systems such as powder nanorods and nanoparticles can be explained by the Kubelka−Munk (KM) theory.[40,41] KM theory is expressed by the following equation.

$$(1 - R_\infty)^2/2R_\infty = F(R) = K/S \qquad (1)$$

K is the absorption coefficient, S is the scattering coefficient, R_∞ is the reflectance of the sample at infinite thickness, and $F(R)$ is the KM function. Kubelka−Monk theory shows that diffuse reflectance from a thick powder starts at unity when the absorption is zero and then falls monotonically with an increase in the ratio of absorption to scattering, K/S, and the rate of fall decreases with increasing K/S. To lowest order scattering, S, increases with increasing real part, and absorption, K, increases with increasing imaginary part of the complex refractive index of the material; the complex refractive index is shown by eq 2.[42]

$$m = n + ik \qquad (2)$$

where 'n' and 'k' are real and imaginary parts of complex refractive index (m) respectively, 'i' is an imaginary number.

Figure 15 shows reflectance measurements for a variety of the samples described herein. Plots (a) and (b) show results for CuO rods with dimension on the order of a couple of micrometers, shown in Figures 7b and 6e, respectively. Reflectances are uniformly large above a wavelength $\lambda \approx 960$ nm but show a rapid drop for shorter λ. CuO is a semiconductor with a band gap of 1.2 eV which corresponds to $\lambda_{gap} = 1030$ nm. Thus, we expect for $\lambda > \lambda_{gap}$ that the CuO is an insulator with a negligible imaginary part of the refractive index; hence, small K leading to large reflectance, whereas for $\lambda < \lambda_{gap}$ CuO is a conductor with large imaginary part of the refractive index; hence, large K leading to small reflectance, and plots (a) and (b) in Figure 15 can be explained on this basis. However, it is remarkable that the known band gap value is 7% larger in λ than observed here, a discrepancy that we cannot explain. Plot (d) in Figure 15 is for CuO nanoparticles on the order of 8−10 nm in diameter, shown in Figure 13a. The reflectance is significantly different than for the same composition, CuO, in plots (a) and (b) to imply the particle morphology is the cause of the difference. Small particles can provide a textured surface with many reflectances leading to large effect on K (eq 1). Overall the reflectance is smaller with smaller λ, consistent with the semiconductor interpretation given for (a) and (b). However, the implied band gap is diffuse, possibly due to a particle size distribution. Moreover, small semiconductor particles typically have higher energy, blue-shifted band gaps relative to the bulk. Plot (d) in Figure 15, if anything, tends to show a redder, lower-energy band gap, which is not clear to explain.

Plot (e) in Figure 15 is for CuO porous particles shown in Figure 12a,b. The reflectance is uniformly low with the band gap onset at around 970 nm. The overall size of particles is ~3 μm, but the porosity makes the spheres rough. To explain the low reflectance, we propose that the surface roughness causes an enhanced absorption K even though the refractive index for $\lambda > \lambda_{gap}$ is mostly real. This roughness-enhanced K causes the reduced diffuse reflectance. This is similar to the texture argument for small particles given above. In the same way, we explain the diffused reflectance curve, plot (h) in Figure 15, for commercial bulk CuO as shown Figure 14a,b; commercial CuO has more surface roughness with particle size from a couple of micrometers to several micrometers. Plot (f) in Figure 15 is for Cu porous spherical particles as shown in Figure 12c,d. Copper is a metal with a large imaginary part to the complex refractive index; hence, large K leading to small reflectance, as observed. It is interesting that plot (f) is very similar to plot (e) for CuO which was explained by surface roughness-enhanced K. The similarity implies that surface roughness is more important than the imaginary refractive index in this case. Plot (g) in Figure 15 is for Cu nanoparticles on the order of 8−10 nm in diameter, shown in Figure 13b. The reflectance is low, consistent with a large K due to the metallic, imaginary refractive index, Cu. Plot

(i) in Figure 15 is for Cu rods with dimension on the order of a few micrometers, shown in Figure 11d,e. Once again, the reflectance is low, consistent with a large K due to the metallic imaginary refractive index.

Furthermore, nanorods were randomly oriented; in addition to morphology, size, refractive indices, and surface texture, diffuse reflectances of CuO/Cu nanorods might possibly depend on their orientation. In randomly oriented rods, there will be more inner space so that NIR will penetrate the layer of the samples, and the direction of the radiation will be changed each time when it strikes a boundary within the sample, possibly leading to more interaction (scattering or absorption).[34,39,41] From the experimental data (Table 2 and Figure 15), CuO nanorods showed more diffuse reflectance, whereas Cu nanorods showed less diffuse reflectance (more absorption), and this result could possibly be related to orientation of these nanorods.

These data improve our empirical knowledge of diffuse reflectance properties of various CuO and Cu nanomaterials with different shapes and sizes. At this point, we are not able to theoretically model these materials but hope to delve into this area in the future.

4. Conclusion

CuO nanorods were synthesized by hydrothermal synthetic routes under novel physical and chemical conditions. The size, morphology, and dimensions of these nanorods were significantly affected by a physical and chemical parameters. These CuO nanorods were reduced to Cu nanorods by 4% hydrogen diluted in helium at elevated temperature. Furthermore, CuO porous particles (2−3.7 μm) and CuO nanoparticles (8−10 nm) were also reduced by the 4% dilute H_2 to metallic copper particles at the same conditions. The morphology of the CuO nanomaterials after reduction was preserved in the form of metallic Cu. The CuO and Cu nanomaterials were employed for diffuse reflections at NIR region. From the comparative study, we found that CuO nanorods exhibited high NIR diffuse reflectance due to the large real (mathematical) part of the complex refractive index. However, normal micrometer scale CuO particles, and Cu nanomaterials with different morphologies demonstrated low NIR diffuse reflectance. The low NIR diffuse reflectance by relatively large CuO particles is attributed to their rough surface so as to absorb NIR; the low diffuse reflectance of Cu nanomaterials is attributed to the large imaginary (mathematical) part of the complex refractive index of copper metal. The high diffuse reflectance of NIR by CuO nanorods suggests that it could have applications as an NIR obscurant.

Acknowledgment. This work was partially funded through the award of a contract from the United States Marine Corps Systems Command to M2 Technologies Inc., KY, and the Army Research Office.

References and Notes

(1) Nickolov, R. N.; Donkova, B. V.; Milenova, K. I.; Mehandjiev, D. R. *Adsorpt. Sci. Technol.* **2006**, *24*, 497.
(2) Khanna, P. K.; Gaikwad, S.; Adhyapak, P. V.; Singh, N.; Marimuthu, R. *Mater. Lett.* **2007**, *61*, 4711.
(3) Yang, Z.; Xu, J.; Zhang, W.; Liu, A.; Tang, S. *J. Solid State Chem.* **2007**, *180*, 1390.
(4) Wen, X.; Xie, Y.; Choi, C. L.; Wan, K. C.; Li, X.; Yang, S. *Langmuir* **2005**, *21*, 4729.
(5) *Nanoscale Materials in Chemistry*; Klabunde, K. J., Ed.; Wiley: New York, 2001.
(6) *Nanoscale Materials*; Liz-Marzán, L. M.; Kamat, P. V. Kluwer Academic Publisher: MA, 2003.
(7) Qi, J. Q.; Tian, H. Y.; Li, L. T.; Chan, H. L. W. *Nanoscale Res. Lett.* **2007**, *2*, 107.
(8) Son, D. I.; Ho, Y. C.; Kim, T. W. *Appl. Surf. Sci.* **2009**, *255*, 8794.
(9) Chen, L. J.; Li, G. S.; Li, L. P. *J. Therm. Anal. Calorim.* **2008**, *91*, 581.
(10) Zhou, K.; Wan, R.; Xu, B.; Li, Y. *Nanotechnology* **2006**, *17*, 3939.
(11) Jiang, X.; Herricks, T.; Xia, Y. *Nano Lett.* **2002**, *2*, 1333.
(12) Wang, W.; Zhan, Y.; Wang, G. *Chem. Commun.* **2001**, *8*, 727.
(13) Xiao, H.; Zhu, L.; Liu, X.; Fu, S. *Solid State Commun.* **2007**, *141*, 431.
(14) Kumar, A.; Srivastava, A. K.; Tiwari, P.; Nandedkar, R. V. *J. Phys.: Condens. Matter* **2004**, *16*, 8531.
(15) Wang, X.; Xi, G.; Xiong, S.; Liu, Y.; Xi, B.; Yu, W.; Qian, Y. *Cryst. Growth Des.* **2007**, *7*, 930.
(16) Zhu, J.; Bi, H.; Wang, Y.; Wang, X.; Yang, X.; Lu, L. *Mater. Lett.* **2007**, *61*, 5236.
(17) Zhang, X.; Guo, Y.; Liu, W.; Hao, J. *J. Appl. Phys.* **2008**, *103*, 114304–1.
(18) Monson, C. F.; Woolley, A. T. *Nano Lett.* **2003**, *3*, 359.
(19) Chang, Y.; Lye, M. L.; Zeng, H. C. *Langmuir* **2005**, *21*, 3746.
(20) Tung, H.; Song, J.; Dong, T.; Hwang, W.; Chen, I. *Cryst. Growth Des.* **2008**, *8*, 3415.
(21) Panigrahi, S.; Kundu, S.; Ghosh, S. K.; Nath, S.; Praharaj, S.; Basu, S.; Pal, T. *Polyhedron* **2006**, *25*, 1263.
(22) Yang, G. X.; Chen, S.; Zhao, S.; Li, D.; Houyim, D. *J. Serb. Chem. Soc.* **2003**, *68*, 843.
(23) Liu, Z.; Bando, Y. *Adv. Mater.* **2003**, *5*, 303.
(24) Qi, L.; Ma, J.; Shen, J. *J. Colloid Interface Sci.* **1997**, *186*, 498.
(25) Zhu, H.; Zhang, C.; Yin, Y. *Nanotechnology* **2005**, *16*, 3079.
(26) Dhas, N. A.; Raj, C. P.; Gedanken, A. *Chem. Mater.* **1998**, *10*, 1446.
(27) Lee, Y.; Choi, J.; Lee, K. J.; Stott, N. E.; Kim, D. *Nanotechnology* **2008**, *19*, 415604–1.
(28) Mamun, M. A.; Kusumoto, Y.; Muruganandham, M. *Mater. Lett.* **2009**, *63*, 2007.
(29) Grouchko, M.; Kamyshny, A.; Ben-Ami, K.; Magdassi, S. *J. Nanopart. Res* **2009**, *11*, 713.
(30) Appleyard, P. G. *J. Opt. A: Pure Appl. Opt.* **2007**, *9*, 278.
(31) Singh, A.; Avachat, S. G.; Singh, H. *J. Sci. Ind. Res.* **1994**, *53*, 667.
(32) Shi, J. M.; Chen, L. L.; Ling, Y. S.; Lu, Y. *Int. J. Infrared Millimeter Waves* **1998**, *19*, 1671.
(33) Shi, J. M.; Wang, J. Y.; Xu, B.; Wang, J. C.; Yuan, Z. C. *Int. J. Infrared Millimeter Waves* **2003**, *24*, 2007.
(34) Jeevanandam, P.; Mulukutla, R. S.; Philips, M.; Chaudhari, S.; Erickson, L. E.; Klabunde, K. J. *J. Phys. Chem. C* **2007**, *111*, 1912.
(35) Kim, J. Y.; Hanson, J. C.; Frenkel, A. I.; Lee, P. L.; Rodriguez, J. A. *J. Phys.: Condens. Matter* **2004**, *16*, 3479.
(36) Zhang, X.; Zhang, D.; Ni, X.; Song, J.; Zheng, H. *J. Nanopart. Res.* **2008**, *10*, 839.
(37) Hong, Z.; CaO, Y.; Deng, J. *Mater. Lett.* **2002**, *52*, 34.
(38) Kelly, K. L.; Coronado, E.; Zhao, L. L.; Schatz, G. C. *J. Phys. Chem. B* **2003**, *107*, 668.
(39) Pasikatan, M. C.; Steele, J. L.; Spillman, C. K.; Haque, E. *J. Near Infrared Spectrosc.* **2001**, *9*, 153.
(40) *Reflectance Spectroscopy: Principle, Methods, and Application*; Körtum, G. Springer-Verlag: New York, 1969.
(41) Lagorio, M. G. *J. Chem. Educ.* **2004**, *8*, 1607.
(42) Appleyard, P. G.; Davies, N. *Opt. Eng.* **2004**, *43*, 376.
(43) GuO, X.; Mao, D.; Lu, G.; Wang, S.; Wu, G. *J. Catal.* **2010**, *271*, 178.
(44) Rodriguez, J. A.; Kim, J. Y.; Hanson, J. C.; Perez, M.; Frenkel, A. I. *Catal. Lett.* **2003**, *85*, 247.
(45) Wan, L.; Cui, X.; Chen, X.; Shi, J. *Mater. Lett.* **2010**, *64*, 1379.
(46) Horns, A.; Hungria, A. B.; Bera, P.; Camara, A. L.; Fernandez-Garcia, M.; Martinez-Arias, A.; Barrio, L.; Estrella, M.; Zhou, G.; Fonseca, J. J.; Hanson, J. C.; Rodriguez, J. A. *J. Am. Chem. Soc.* **2010**, *132*, 34.
(47) Pedersen, D. B.; Wang, S. *J. Phys. Chem. C* **2007**, *111*, 17493.
(48) Duan, J. L.; Cornelius, T. W.; Liu, J.; Karim, S.; Yaho, H. J.; Picht, O.; Rauber, M.; Muller, S.; Neumann, R. *J. Phys. Chem. C* **2009**, *113*, 13583.
(49) Willets, K. A.; Duyne, R. P. V. *Annu. Rev. Phys. Chem.* **2007**, *58*, 267.

JP103761H